Biophysical Journal Volume 96 April 2009 2789–2798

Interfacial Water at Protein Surfaces: Wide-Line NMR and DSC Characterization of Hydration in Ubiquitin Solutions

Kálmán Tompa,[†] Péter Bánki,[†] Mónika Bokor,[†] Pawel Kamasa,[†] György Lasanda,[†] and Péter Tompa[‡*]
[†]Research Institute for Solid State Physics and Optics, and [‡]Institute of Enzymology, Biological Research Center, Hungarian Academy of Sciences, Budapest, Hungary

ABSTRACT Wide-line ^{1}H-NMR and differential scanning calorimetry measurements were done in aqueous solutions and on lyophilized samples of human ubiquitin between −70°C and +45°C. The measured properties (size, thermal evolution, and wide-line NMR spectra) of the protein-water interfacial region are substantially different in the double-distilled and buffered-water solutions of ubiquitin. The characteristic transition in water mobility is identified as the melting of the nonfreezing/hydrate water. The amount of water in the low-temperature mobile fraction is 0.4 g/g protein for the pure water solution. The amount of mobile water is higher and its temperature dependence more pronounced for the buffered solution. The specific heat of the nonfreezing/hydrate water was evaluated using combined differential scanning calorimetry and NMR data. Considering the interfacial region as an independent phase, the values obtained are 5.0–5.8 $J \cdot g^{-1} \cdot K^{-1}$, and the magnitudes are higher than that of pure/bulk water (4.2 $J \cdot g^{-1} \cdot K^{-1}$). This unexpected discrepancy can only be resolved in principle by assuming that hydrate water is in tight H-bond coupling with the protein matrix. The specific heat for the system composed of the protein molecule and its hydration water is 2.3 $J \cdot g^{-1} \cdot K^{-1}$. It could be concluded that the protein ubiquitin and its hydrate layer behave as a highly interconnected single phase in a thermodynamic sense.

INTRODUCTION

Our long-range goal is to understand better, using a multiexperimental approach, the structure and dynamics of the protein-water (protein-solvent) interfacial region and its relationship with protein structure and function. From the rich literature about protein hydration, a few reviews are invoked here as an introduction to the field. Cooke and Kuntz (1) give a general introduction and definitions of the quantities used. Rupley and Carreri (2) deal mainly with powder samples of different water content. Finally, Simonson (3) gives an introduction to the electrostatics and dynamics of aqueous solutions, which provides an overview of the history and evolution, as well as results on globular protein-water interfacial regions. The state of the art and the still open questions have been described in several recent articles as well (see, for instance, (4–7) and references therein). The experimental research was critically summarized by Halle (4), with the main diagnostic (somewhat pessimistic) conclusions that ''the progress is less and erratic, and the results given by different experimental methods are contradictory and more or less model-dependent in the interpretation''. He proposed the application of the nuclear magnetic relaxation dispersion technique as a therapy in this situation.

A cross section of the molecular dynamics simulation (MDS) field has been surveyed by Bizzarri and Cannistraro (6), who point out that the analysis of the number of different water molecules engaged in protein-solvent H-bonds provides information about the dynamics of the H-bond network at the protein-solvent interface. In addition, it was found that the number of these water molecules exhibits a critical transition at about −73 to −53°C (see, e.g., (8,9)). In hydrated proteins, at about −53°C, the amplitude of atomic motion suddenly becomes enhanced, signaling the onset of more ''liquidlike'' motion. This solvent-driven ''dynamical transition'' of proteins (9) may be triggered by coupling of the protein with the hydrate water through hydrogen-bonding, since hydrate water of proteins shows a dynamic transition at a similar temperature. Below this temperature, conformational transitions are kinetically arrested, and above it, molecular motions start. A similar strong coupling between motions of protein and its hydrate layer has been reported recently in the case of endoglucanase III (10), where heat capacity of the protein-water system was directly calculated from MD simulations (8.46 ± 0.15 $J \cdot g^{-1} \cdot K^{-1}$). The dynamic transition was attributed to the relaxation of the H-bond network via translational displacements of solvent molecules.

These and other observations, and the modeling of water structure and dynamics, suggest that several questions regarding the protein-hydrate interface are unresolved, i.e., experimental investigation of the hydration properties of proteins is more active than ever (11). Furthermore, it has thus far been considered unimportant that many proteins and/or protein domains lack a well-defined structure under native conditions (12,13), that is, that they are intrinsically disordered/unfolded proteins. Due to their increased level of flexibility and hydration (12,14–16), structural and dynamical description of their protein-water interfacial region represents a novel and pressing challenge for theoreticians and experimentalists alike.

Our long-range goal is to characterize in detail the interfacial water of intrinsically disordered or unfolded proteins and

Submitted June 24, 2008, and accepted for publication November 10, 2008.

*Correspondence: tompa@enzim.hu

Editor: Bertrand Garcia-Moreno.

0006-3495/09/04/2789/10 $2.00

doi: 10.1016/j.bpj.2008.11.038

globular proteins (as reference materials) with the aim of developing an approach based on wide-line NMR spectrometry, nuclear relaxation time measurements, and differential scanning calorimetry (DSC). This multiexperimental approach makes it possible to identify novel intrinsically disordered proteins and to characterize the differences between the two classes of proteins. For a comprehensive treatment of the field up to 1982, and to better assess the consequences of extending our research to subzero temperatures, the reader is referred to the monograph of Derbyshire (17).

The use of water mobility (the NMR-visible proton motion) as a key factor for distinguishing water fractions was initiated by Kuntz (18,19). The methodical details applied by Kuntz were later criticized by Derbyshire because 1), his determination of the number of contributing nuclei is burdened by the greater inherent error of applying the continuous-wave NMR technique instead of the pulse technique; 2), he chose only a single temperature below the bulk freezing point at which the signal is recorded; and 3), a separate and chemically different standard was applied for the normalization of the number of contributing nuclei (17). Our approach, which avoids these pitfalls, will be described later in this study. Iin our previous work, we applied this approach using bovine serum albumin (BSA) as a reference protein (14,15,20), whereas human ubiquitin is our candidate in this work, for several reasons. First, there is a thorough MDS work of Schröder and co-workers (5) on the protein-water interface (hydration size, mean residence time, etc.) of three globular proteins including ubiquitin (Protein Data Bank entry 1UBQ). Some of their results, and the data on the molecular characteristics, are reproduced here for convenience. 1UBQ is a small, more or less spherical protein found in all eukaryotic cells and is used for labeling misfolded/damaged proteins destined for degradation in the cell. 1UBQ is also used for other tasks, such as directing the transport of proteins in and out of the cell. Some of its physical-chemical characteristics are a molecular mass of 8565 g/mol, a solvent-accessible surface area (5) of 5321 $Å^2$, and a charge of 0 q/e. In addition, it has 29 amino acids (out of a total of 76 amino acids) that fulfill the solvent-accessibility criterion (5), and 150 hydrogen atoms that belong to methyl groups (24% of 629 total H-atoms,) and 210 that belong to methylene groups (33% of the total H-atoms).

In our research, a novel combined experimental approach has been applied (14,15,20). This interface-oriented approach combines cooling and step-by-step reheating technology, and applies pulsed wide-line NMR and supplementary DSC measurements. This approach connects microscopic and macroscopic methods, and it is not reduced to the ''solid state'' of the dry/water-free or frozen samples. Wide-line NMR applies several different pulse-excitation techniques, and measures nuclear magnetization, free induction decay signal, and echoes (21–24) in response to the excitation. Nuclear magnetization is in direct proportion to the number of nuclei contributing directly to the specific NMR response. The free induction decay signal is the inverse Fourier transform of the NMR spectrum. In a heterogeneous sample (or, in the language of NMR people, ''in a multifraction spin system''), the response contains global information on the total spin system, and also on any of its fractions. In our case, the distinction of H_2O fractions is based on the differences in their water/proton mobility, as detected on the basis of the ''motional narrowing'' phenomenon (25,26). The interproton dipole-dipole interaction is dominant in an immobile ^{1}H-nuclear-spin system and makes the NMR lines a few 10 kHz wide. The motional narrowing averages out (partly or totally) the dipole-dipole interaction and manifests in narrow ^{1}H-NMR lines on the frequency scale. Here, immobility means the absence of reorientation or translation while lattice vibrations are active. The term ''mobile'' for the purposes of this article denotes that the species in question are visible by NMR and are mobile on the timescales of NMR.

The physical reduction in sample heterogeneity and response complexity is achieved by changing the temperature and/or by the proper selection of radiofrequency pulse excitation (27), respectively. Further, the low-temperature (below 0°C) mobile water fraction is identified as interfacial water, and thus, the size, dynamics, and evolution of the hydration shell can be investigated as a function of temperature.

This approach separates not mathematically but physically the different fractions in the examined complex system. In our aqueous solutions, the molecular motion of water starts in the temperature range determined by the critical transition of hydration water (6,8,9) and by the dynamical transition of protein (9,28) for all of our investigated (published or to be published) protein-water systems (14,15,20). The understanding of the correlation between the thermal history of the nonfreezing/mobile water and the calculated quantities (6,28) represents a challenge that promises a more thorough description of the structure and dynamics of hydrate water (to be published in a separate article).

MATERIALS AND METHODS

Samples

Lyophilized ubiquitin (UBQ) was obtained from Sigma Chemical (St. Louis, MO), and either used as delivered by the supplier (''powder'') or dissolved in pure water (Millipore, Billerica, MA) or buffer (50 mM Tris, 150 mM NaCl, and 1 mM EDTA). The two different solvents were selected to study the effects of the NaCl cosolute. The water content of the 1UBQ powder sample was determined from the ^{1}H-NMR signal intensity, and a hydration of $h = 0.145$ g water/g protein (12.7 wt %) was found.

Because the NMR and DSC experiments to be carried out consist of reversible freezing and drying of the UBQ solution, it is important to ensure that protein integrity is maintained by stability of UBQ under these conditions. In general, UBQ is known to be a very stable protein that cannot be cold-denatured without the addition of denaturants (36). In addition, our observations could be reproduced after several rounds of freeze-thaw cycles. Furthermore, we carried out two additional tests to make sure that our protein in solution gets neither unfolded nor aggregated under the experimental conditions. Unfolding has been excluded by recording the circular dichroism spectrum of UBQ in the above buffer at room temperature, after

a freeze-thaw cycle, and after 60°C × 10 min treatment. The three spectra are practically indistinguishable, attesting to the theory that UBQ is resistant against unfolding at both low and high temperatures. To exclude the possibility of aggregation of the sample, absorbance of UBQ solution was measured under the above three conditions (i.e., room temperature, after a freeze-thaw cycle, and after heat treatment). The three absorbance values measured at 400 nm are close to zero under all three conditions, i.e., there is no discernible aggregation under the experimental conditions to be used.

NMR spectrometry

At this point, it is necessary to repeat some basic elements of NMR spectrometry. The nuclear dipoles sample the local magnetic fields, but the responses of the nuclear spin system are specific ones depending on the form of the radio-frequency excitation. The details of this case, where the protons in protein-water systems constitute the nuclear spin system, are given in Tompa et al. (27) and references cited therein). Free induction decay (FID), "solid echoes" (24), the amplitude of the FID signal, and the Carr-Purcell-Meiboom-Gill (CPMG) echoes (22,23) were measured in the temperature range between −70°C and +45°C. The measurements were realized at thermal equilibrium at every temperature, and data acquisition was started when the NMR response became time-independent, which usually took ~10 min. Measurements were made while cooling and while heating the samples. The cooling data branch can be burdened by the effects of supercooling, but data recorded while heating are free from such phenomena and are considered as taken in thermal equilibrium. The protein solutions showed no thermal hysteresis or signs of supercooling below the freezing point of bulk water. The data presented are those obtained while heating, unless stated otherwise.

The portion of mobile proton (water) fraction was measured directly by two ^{1}H NMR methods, by recording 1), the FID signal; and 2), CPMG-echo trains (in the temperature range where echoes existed at all). Determination of the mobile water fraction is based on a comparison of the signal intensity or echo amplitude extrapolated to $t = 0$ with the corresponding values measured at a temperature where the whole sample is in the liquid state. The extrapolated amplitude of the CPMG-echo train at $t = 0$ gives the portion of mobile protons (25,26). as does the extrapolated FID amplitude sampled from 200 μs to infinity. The zero-time signal intensity or echo amplitude is proportional to the number of mobile resonant nuclear spins in the sample. These quantities depend on the nuclear magnetization given by the standard formula as $M_i \propto N_i B_0/T$, where B_0 is the static magnetic induction, N_i is the number of contributing nuclei, and T is the absolute temperature. The signal detected in the time interval from zero to 200 μs is a mixture of transient signals over the dead-time period of the spectrometer with some remaining parts of ice and protein FID signals. The points measured during this period were omitted, but the top part of the solid echo completes the missing part of FID. The two methods (extrapolated amplitudes of the FID signal or the CPMG-echo train) gave exactly the same results at all the temperatures where mobile protons (mobile water molecules) exist, and the evolution of mobile (nonfreezing) water fraction during heating has been determined. CPMG echoes can be detected only on nuclei for which the homonuclear dipolar interaction is averaged out by atomic or molecular motions. The completion of FID from the solid echo gives a chance for more precise determination of the second moment for the solid component (which is important for the lyophilized samples).

The mobile water fraction data obtained were also used in the interpretation of the thermal properties measured by DSC techniques. The effect of freezing on the protein solutions was controlled by comparison of the NMR parameters obtained before and after a freeze-thaw cycle at temperatures >0°C. We found that the freeze-thaw cycle caused no observable changes for the studied samples as far as the measured NMR parameters are concerned. The temperature was controlled by an open-cycle Oxford cryostat with an uncertainty $> \pm 1$ K. ^{1}H NMR measurements and data acquisition were accomplished by a Bruker SXP 4-100 NMR pulse spectrometer at frequencies of 82.6 MHz with a stability of better than $\pm 10^{-6}$. This value represents the stability of the electromagnet, without any drift during measurements; the stability of the frequency is better for our system by two orders of magnitude. The data points in the figures are based on spectra recorded by averaging signals to reach a signal/noise ratio of 50. The number of averaged NMR signals was varied to achieve the desired signal quantity for each sample and for unfrozen water quantities. To determine the relative number of mobile protons, the sensitivity of the NMR spectrometer to temperature change was controlled by measuring the length of the $\pi/2$ pulse to obtain reliable M_i values (27). The extrapolation to zero time was done by fitting a stretched exponential.

DSC

The information about structural and dynamic changes of protein and water as solvent can be deduced from the amount of heat absorbed or emitted by a sample subject to controlled temperature change. Among calorimetric methods, DSC is one that allows for precise determination of the enthalpy changes from the recorded temperature difference (29) between the reference and the sample branches, ΔT, as

$$\Delta H = K \int_{t_1}^{t_2} \Delta T \mathrm{d}t. \quad (1)$$

Once the calorimeter constant, K, is calibrated, the heat flow, $\mathrm{HF} = K \times \Delta T$, and the associated specific heat at constant pressure, c_{p}, of a sample of mass m can be determined at a given heating rate, q, as

$$c_{\mathrm{p}} = \frac{\mathrm{HF}}{m \times q}. \quad (2)$$

The enthalpy associated with the specific heat is overlapped with much greater enthalpies of phase transitions when such take place. If the heat capacities are known, enthalpies of transitions can be separated. For the measurements, a TA Instruments (New Castle, DE) heat-flux-type DSC 2920 cell was employed (30). The measurements were carried out at heating controlled with a rate of 2 K·min^{-1}.

RESULTS AND DISCUSSION

Lyophilized protein samples: FID, echoes, and frequency domain spectra

The room-temperature time-domain FID and echo signals measured on 1UBQ powder are comprised of a fast and a slow component (Fig. 1). The fast component comes from the solid parts of the sample. These parts—the protein molecules—are immobile from the point of view of NMR. The protein molecules undergo no translation or reorientation as a whole; however, some reorientation motions of small molecular groups of the amino acid side chains are detected in this state. The long tail is the response of mobile protons of the nonfreezing water in the sample. The nonfreezing phase represents reorienting water molecules. The initial ($t = 0$) amplitudes of these components are proportional to the number of ^{1}H nuclei in the relevant parts of the sample (see Materials and Methods). The ratio of the two components gives the measure of water content in the manufacturer-delivered sample, $h = 0.145$ (12.7 wt %). The water content of the powder sample is well below the limit required for biological functioning or for full water coverage. It is believed that $h = 0.2$–0.4 is sufficient to cover most of the protein surface with a single layer of water

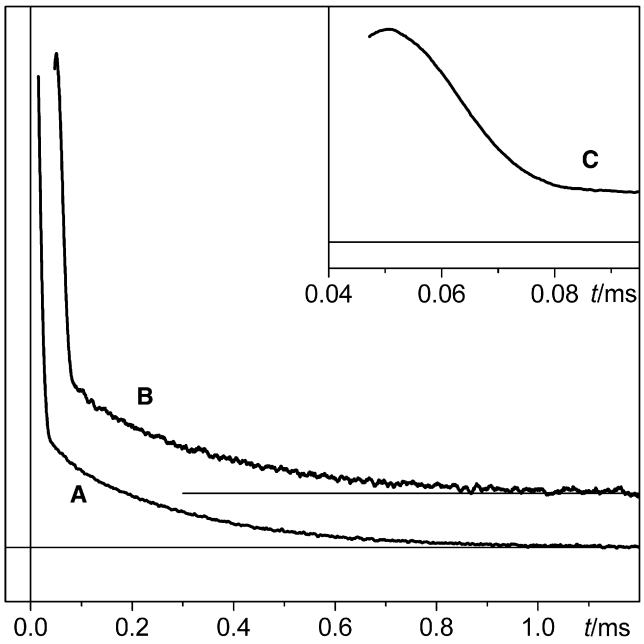

FIGURE 1 ^{1}H-NMR signals for ubiquitin powder at room temperature. (*A*) FID signal. (*B*) $(\pi/2)_X - \tau - (\pi/2)_Y$ – echo signal (shifted vertically). (*C*) The central part of the range described in *B*.

molecules and to fully activate the protein functionality (31,32). The water origin of the signal is proved by the temperature dependence of such signal parameters as spectrum width and intensity (Fig. 2). The Fourier transform of the time-domain long tail corresponds to a narrow line in the frequency domain. The full width at half maximum of the narrow line, FWHM = 1.2 kHz = 0.27×10^{-4} T, is greater than that of hydration shell protons measured at low temperatures (see Aqueous solutions: NMR spectra). The mobility of the water molecules in the lyophilized sample is more restricted (wider spectrum) than in the first hydration shell at low temperatures (narrower spectrum). The lack of this narrow line at about −70°C is characteristic of the stopping of proton (water molecule) reorientation. The broad spectrum (short component in the time domain) allows us to determine the second moment, M_2, for protein protons. The estimated value from the second derivative of the relevant solid-echo component (22,23) is $M_2 = 7.20 \times 10^3$ kHz^2 = 10.1×10^{-8} T^2 at 23°C. This M_2 value refers to rotation around a symmetry axis performed by high-symmetry molecular groups (e.g., methyl), which becomes obvious when the second moments for a rotating and an immobile methyl group are compared. The intramolecular M_2 contribution of immobile methyl groups is 1.63×10^4 kHz^2 = 22.8×10^{-8} T^2, which is reduced by a factor of 0.25 by the rotation about the C_3 symmetry axis of the group (33). The water protons in mobile water give a substantially narrower line, FWHM <1 kHz, and a second moment that is <0.18 kHz^2 = 2.5×10^{-12} T^2. The water protons in a rigid (static) water molecule give a line of FWHM ~ 40 kHz and a second moment of ~1.1×10^4 kHz^2 = 16×10^{-8} T^2.

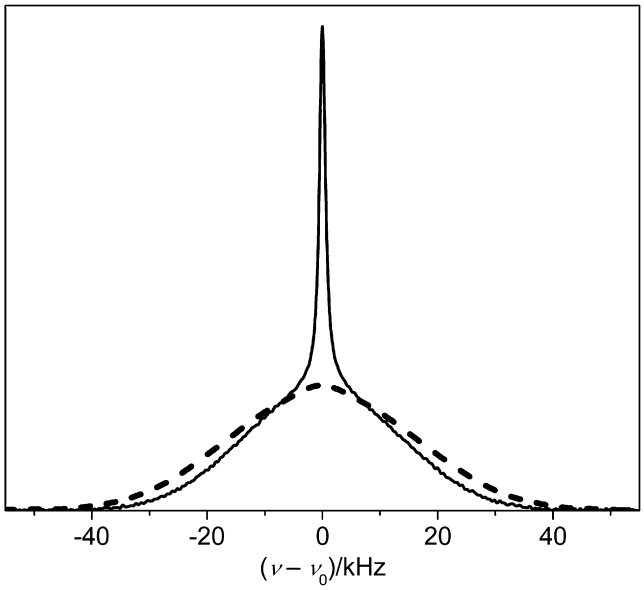

FIGURE 2 ^{1}H-NMR spectra for ubiquitin powder at +24.8°C (*solid line*) and–74.5°C (*dashed line*).

The second moment values obtained were found to correspond to rotating methyl and possibly to reorienting methylene groups. This is in accordance with the conclusions of Russo et al. (34) who used elastic and quasielastic neutron scattering experiments to investigate the dynamics of methyl groups in a protein-model hydrophobic peptide in solution. Their results proved that a hydrophobic side chain requires more than a single layer of solvent to attain the liquidlike dynamical regime. They showed that when hydrophobic side chains are hydrated by a single water layer, the only allowed motions are attributed to simple rotations of methyl groups. Our result is supported by the MDS of Curtis et al. (35), which proved that water is required for the methyl groups to exhibit the full range of motion characteristic of the liquidlike protein state at room temperature. Their study provided direct evidence that both the amplitude and distribution of motion are influenced by the solvent and are not exclusively intrinsic properties of the protein molecule itself.

DSC and the NMR line widths of the broad component (Fig. 2) on powder samples give a smooth curve (without any small extra peaks or steps, respectively, characteristic of phase transformation), demonstrating that neither cold denaturation (36) nor other phase changes play any role in the temperature range investigated. This is also confirmed by the DSC and NMR amplitude versus temperature curve on aqueous solutions (see below).

Aqueous solutions

NMR intensities

The wide-line ^{1}H-NMR signal intensity is the measure of the number of mobile protons or, equivalently, the number of

mobile water molecules. We converted the measured signal intensities into the fractions $x = n$(mobile H)/n(total H) for water (Fig. 3 *A*, *triangles*), buffer (Fig. 3 *B*, *triangles*), ubiquitin dissolved in water (Fig. 3 *A*, *circles*), and ubiquitin dissolved in buffer (Fig. 3 *B*, *circles*). The concentrations corresponding to the water amounts in the first and in the first and second hydration shells of ubiquitin, calculated by molecular dynamics simulations (5), are also shown (*dashed lines*). The hydration level corresponding to $h = 0.4$ ($x = 0.016$) is shown for comparison (*dash-dotted lines*).

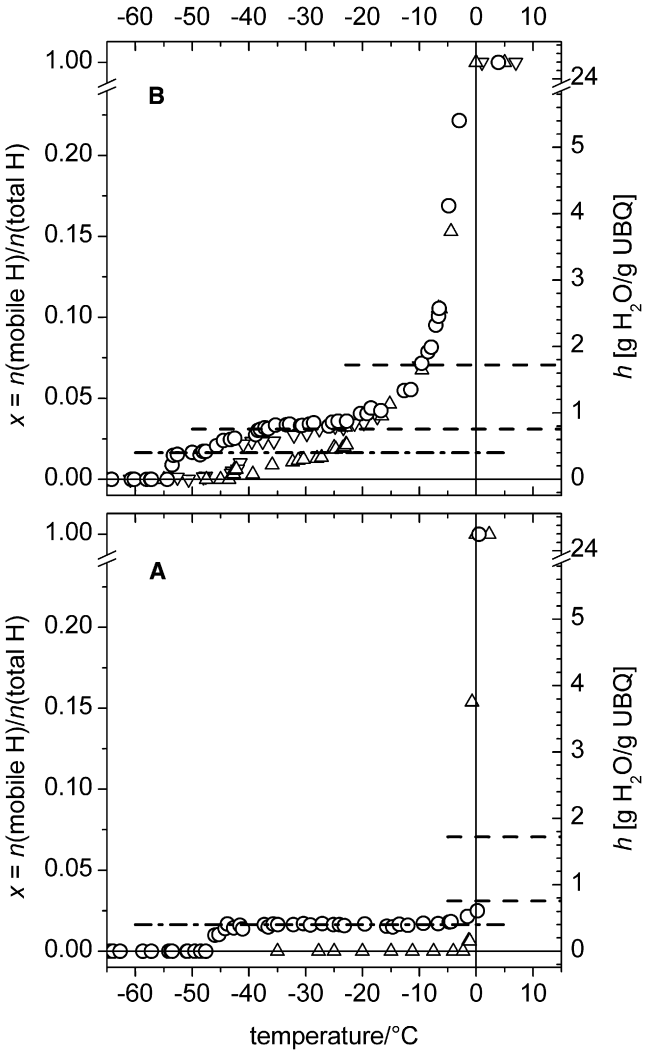

FIGURE 3 Mobile water fractions $x = n$(mobile H)/n(total H) determined from ^{1}H-NMR signal intensities for (*A*) 41 mg/cm^3 ubiquitin dissolved in water (*circles*) and pure water (*triangles*), and (*B*) 41 mg/cm^3 ubiquitin dissolved in room temperature buffer (*circles*), buffer measured while cooling (*inverted triangles*), and buffer measured while heating (*triangles*). Concentrations corresponding to the water amounts in the first, and in the first two, hydration shells of ubiquitin calculated by molecular dynamics simulations (5) (*dashed lines*) are $x(1) = 0.0310$ ($h(1) = 0.756$) and $x(1 + 2) = 0.0705$ ($h(1 + 2) = 1.72$); the hydration level, $h = 0.4$ g/g protein ($x = 0.016$), is marked by dash-dotted lines. For comparison, the scales for hydration (h) are also given (right axes of ordinates).

The mobile water fraction, x, is zero for up to 0°C in the water sample (Fig. 3 *A*), i.e., molecular motion starts at the melting point of (hexagonal) ice in the whole sample. The mobile water fractions for water (Fig. 3 *A*) and for buffer (Fig. 3 *B*) samples (without protein solute) demonstrate characteristic differences between the two solvents.

The x versus T data show a step for 1UBQ in water at about −45°C (Fig. 3 *A*), suggesting that detectable molecular motion starts at this temperature. The molecular motion is probably the rotation of water molecules in the interfacial region. This means that the thermal excitation of ''bound'' (1) water molecules needs a lower energy in the interfacial region than in the hexagonal ice! The amplitude of the signal remains unchanged up to the melting point, where the whole sample melts, i.e., x becomes equal to 1 ($h = 24.4$). Two conclusions can be drawn by comparing the measured number of mobile water molecules to the theoretical estimated value (5). The first is that the magnitude of both is in the same order and the measured number of mobile water molecules equals the hydration level corresponding to $h = 0.4$ ($x = 0.016$), required for protein activity. Dehydrated enzymes are not active, but a single layer of water surrounding them restores their activity (32,33). It has been shown that the enzymatic activity of proteins depends crucially on the presence of a minimum amount of solvent water. The second conclusion is that there is no change in the number of mobile water molecules up to the melting point. This fact also demonstrates that there is no change at the molecular surface and consequently no phase transformation in the protein structure in this temperature range.

The x versus T data show a thermal hysteresis for buffer (Fig. 3 *B*) (see details in (14)), whereas no hysteresis is observed in protein-buffer aqueous solutions. The typical phase diagrams for a simple solution of a small-molecular-weight solute and of a macromolecule (17) predict this difference in the thermal behavior. There is a step in the x versus T data of 1UBQ in buffer at about −53°C (Fig. 3 *B*), which suggests that molecular motion in this case starts at this temperature. The molecular motion is probably the rotation of water molecules in the interfacial region. The steps are at −40°C (cooling) and at −25°C (heating) for the buffer. In the whole temperature range below 0°C, there are discernible molecular motions, and the number of mobile water molecules increases with temperature. These observations and the DSC results (see below) suggest that the properties of interfacial water at the surface of the protein are not simply the sum of those of the buffer and those of the protein molecules. The resulting properties reflect to a new protein-buffer complex entity.

The slopes of mobile water fraction versus temperature curves were calculated (Table 1) to give a quantitative parameter characteristic of the heterogeneity of protein-water and protein-buffer-water interactions. These slope values reflect inhomogeneity of the ''landscape'' around protein molecules or protein-buffer complexes. The more heterogeneous these

TABLE 1 Slopes and intercepts of mobile water concentration versus temperature curves for protein solutions below 0°C

Protein/solvent*	UBQ/water	UBQ/buffer	BSA/water	BSA/buffer
Intercept at 0°C	2.22 ± 0.02	7.7 ± 0.2	2.10 ± 0.04	7.28 ± 0.08
Intercept at 0°C	0.355 ± 0.003	1.23 ± 0.03	0.331 ± 0.006	1.15 ± 0.01
T_f/°C	−46	−53	−62	−54
Intercept at T_f	2.22 ± 0.02	2.2 ± 0.1	2.10 ± 0.04	2.38 ± 0.02
Intercept at T_f	0.355 ± 0.003	0.35 ± 0.2	0.331 ± 0.006	0.376 ± 0.003
Slope	0	0.104 ± 0.006	0	0.091 ± 0.002
Slope	0	0.017 ± 0.001	0	0.0144 ± 0.0003

*Values for intercepts are given first in units of n(mobile H_2O)/n(amino acid residue) and then in units of g H_2O/g protein. Values for slopes are given first in units of n(mobile H_2O)/n(amino acid residue)/°C and then in units of g H_2O/g protein/°C.

interactions are, the higher is the slope. Zero slopes correspond to homogeneous interactions. We think that the magnitude of hydration and the slope of the hydration-temperature curve can serve as a static representation of the interfacial landscape around protein molecules.

The temperatures where interfacial water melts (T_f, Table 1) fall within a 16°C range for the examples given. The lowest temperature, −62°C, was found for BSA in water and the highest, −46°C, for 1UBQ in water. This 16°C range corresponds to 133 $J \cdot mol^{-1} = 1.38$ meV on the thermal energy scale, calculated as RT or k_BT.

Our measurement of the constant concentration of mobile water molecules in water solvent is 187 ± 2 mol H_2O/mol 1UBQ at $45°C < T < 5°C$ (Fig. 3 *A*). This hydration value can be compared with the number estimated by the sum of the hydration values of the individual amino acids needed to build the protein molecule. Kuntz proposed amino acid hydrations deduced from continuous-wave NMR experiments for polypeptides at −35°C (18). The application of these numbers gives 200 ± 30 mol H_2O/mol UBQ. Two other works that cite Kuntz's data give somewhat different amino acid hydrations, resulting in 193 ± 29 (17) and 222 ± 47 (22) mol H_2O/mol UBQ. The good agreement between our directly measured hydration and the estimated ones is surprising. The estimation involves the supposition that each amino acid residue in the protein is hydrated as if it were fully exposed to the solvent at the surface of a globular protein i.e., the estimated protein hydration is higher than that measured directly. Kuntz et al. experimented with solutions containing 5–10 wt % protein and 0.01 M KCl. Our results for the hydration of 1UBQ dissolved in buffer (4 wt % protein, 0.150 M NaCl, 0.050 M Tris) are considerably different from those of Kuntz.

The following important questions can be raised when analyzing the results depicted in Fig. 3. 1), What is the actual size of the hydration shell(s)? 2), Why are the hydration properties so different in water and buffered solutions? 3), What is the physicochemical background of the substantial change in the NMR intensity curve for buffered solution at about −20°C? Does this reveal the ''melting'' of the second hydration shell? 4), The change in the slope at about −15 to −10°C means a qualitative change in the motion of water molecules at the protein surface. Why are these two features missing in the solution that is not buffered?

NMR spectra

^{1}H-NMR spectra measured for both ubiquitin solutions are given in Fig. 4. The spectra are Fourier-transformed FID signals on a frequency scale. FWHMs are given for each spectrum. The width of the spectra above 0°C can be taken as a measure of the inhomogeneity of the applied static magnetic induction B_0; the frequency values given correspond to an inhomogeneity up to 2 ppm (0.16 kHz) for our magnet. Going down with the temperature, the spectral component corresponding to interfacial water widens to FWHM = 0.2–0.7 kHz. These measured values show that motional averaging is not as effective in these solutions as in normal liquids, i.e., the motions are restricted. At the lowest temperatures, where there are no water molecular motions (and the signal intensity is very poor), the detected signal comes from the moving end-groups of the protein, and the estimated value of the scale of 10 kHz corresponds roughly to that measured on a lyophilized powder sample. The main result of the direct measurements of wide-line ^{1}H-NMR spectrum widths for interfacial water is the value of 0.2–0.7 kHz. The origin of the broadening is the dipole-dipole interaction (which is not averaged fully by molecular motions), because CPMG echoes do not exist in the whole temperature range, appearing at −26°C for UBQ in water and at −51°C for UBQ in buffer (Fig. 4, *solid stars*) when heating, and translation diffusion starts at −4°C for UBQ in water and at about −10°C for UBQ in buffer (Fig. 4, *open stars*). Detailed measurements on ^{1}H NMR relaxation rates and their analysis will be presented in a forthcoming article.

DSC traces and enthalpy curves

The DSC trace and the corresponding curve of enthalpy change for water (Fig. 5) are determined by the temperature dependence of the specific heat of ice below 0°C. The heat of fusion has a major effect upon melting at 0°C, and then the specific heat of water controls the measured ΔT versus T data, and thus also ΔH versus T. This simple case enables normalization by using the known value of the heat of fusion (enthalpy) of water, $\Delta H_{H2O} = 333.6\ J \cdot g^{-1}$ (37).

We measured the thermal curves of pure water, buffer solution, and 1UBQ dissolved in water and in buffer by DSC (Fig. 5 *upper*). The specific heat of ice determines the

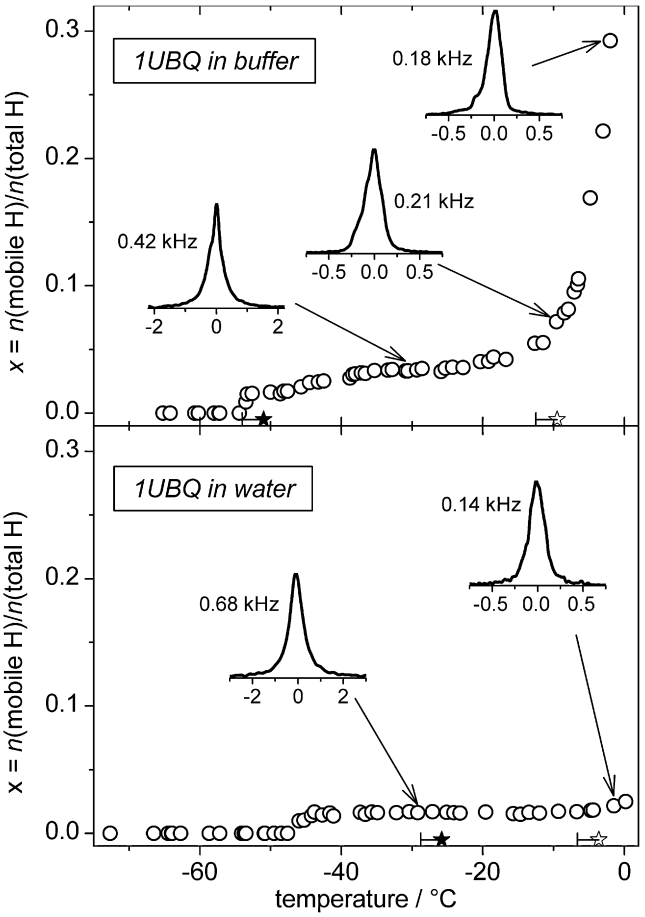

FIGURE 4 ^{1}H NMR spectra and mobile water fractions $x = n$(mobile H)/n(total H) determined from ^{1}H-NMR signal intensities for 41 mg/cm^3 ubiquitin dissolved in buffer (*upper*) and in water (*lower*) . Solid stars denote the lowest temperature where CPMG echoes could be detected and open stars show the lowest temperature where CPMG-echo trains reflected the translational diffusion of (water) protons. Spectra (*inset graphs*) are Fourier-transformed FID signals on the kHz frequency scale. The FWHM is given for each spectrum. The concentrations of mobile ^{1}H nuclei (*circles*) correspond to water molecules in a mobile motional state. The FWHM of the spectra above 0°C can be taken as a measure of the inhomogeneity of the applied static magnetic field, B_0; it is 0.14 kHz for the pure water solution (*lower*) and 0.19 kHz for the buffered solution (*upper*). At low temperatures where the water content is completely frozen, the FWHMs of the spectra are on the scale of 10 kHz for both solvents.

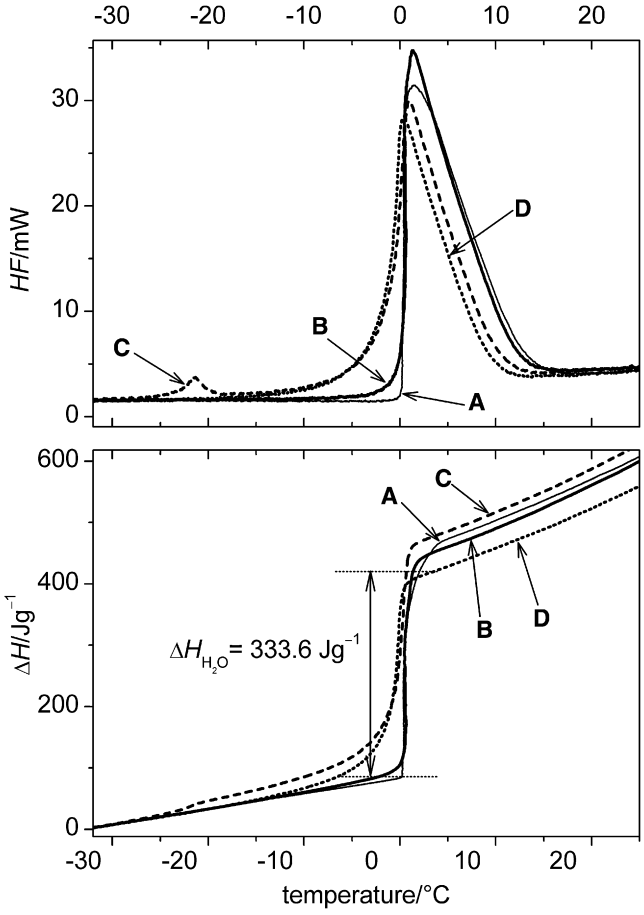

FIGURE 5 (*Upper*) DSC traces for heat flow (HF) versus temperature (T) obtained during heating for (*A*) water, (*B*) 41 mg/cm^3 ubiquitin dissolved in water, (*C*) buffer, and (*D*) 41 mg/cm^3 ubiquitin dissolved in buffer. (*Lower*) Enthalpy change curves calculated from the DSC traces depicted in the upper graph.

ΔT versus T curve of water below 0°C. In this range, the specific heat of ice changes slightly with temperature. At 0°C, water exhibits a rapid increase of ΔT that reflects melting. ΔT returns exponentially to the level determined by the specific heat of the liquid when melting is completed. This is a transient effect that indicates how the sample temperature increases from the melting temperature to the stationary state of any transition. The specific heat of the liquid then determines the level of ΔT. The buffer solution produces two markedly different results (Fig. 5, *line C*) compared with water. There is a small endothermic peak at about –22°C that is caused by the eutectic phase transition (buffer contains 150 mM NaCl) and then ΔT increases continuously up to 0°C due to the heat required to melt the remaining ice. The heat associated with dilution of the crystalline salt in just molten ice during the solid-liquid transition was estimated to be negligibly small, <2% of the heat of eutectic melting (29,38).

The DSC curve of the 1UBQ in water solution (Fig. 5, *line B*) differs only slightly from that of pure water, and the higher ΔT values are caused by a small fraction of water below 0°C (Fig. 3). Greater differences were detected in the case of 1UBQ dissolved in buffer (Fig. 5, *line D*) in conformity with the higher water content below 0°C (Fig. 3).

Nonfreezing water fraction determined by DSC

As a first approximation, we assumed that our systems consist of hexagonal ice and water phases below 0°C. We have a two-phase system this way (we ignore the dissolved protein) and assume that the interfacial water at the surface of the protein has the same thermodynamic properties as bulk water. The fraction of H_2O(l) below 0°C was then calculated from the enthalpy changes as follows. The enthalpy of ice is subtracted

from the total enthalpy of a fractionally melted solution. The result normalized by the enthalpy of ice-to-water transition represents a water fraction in frozen solution:

$$\text{fraction}(H_2O) = \frac{\Delta H_{\text{solution}}(T) - \Delta H_{H_2O}(T)}{\Delta H_{H_2O}}. \quad (3)$$

Fractional melt obtained in this way parallels the $x = n$(mobile H)/n(total H) value obtained from proton intensity measured by the NMR signal intensity (Fig. 6).

For the buffer solution, there is but little systematic difference between the mobile water fraction data measured by NMR and that calculated from ΔH curves (Fig. 6 *C*). We obtained fractional melt values from ΔH above the eutectic temperature that were higher than the x values from NMR; however, the overall trends are the same. For the protein solutions (Fig. 6, *B* and *D*) even the trends are different, except at $T > -15$°C for the buffered 1UBQ solution. These discrepancies point out that the specific heat of the ''liquid'' solution phase differs significantly from that of water. The resulting fractional melt curves (Fig. 6) show the appearance of liquid water at temperatures where lowest-temperature CPMG echoes could be detected by NMR (Fig. 4, *solid stars*). The lowest temperatures where CPMG experiments reflect translational diffusion of mobile protons (Fig. 4, *open stars*) agree well with the temperatures where the fractional melt calculated from the DSC curves and the mobile water fraction obtained from NMR intensities coincide.

Specific heat of hydration water

As a second approximation, we modeled the 1UBQ/water solution taking into account the solvated protein molecules also. The mobile water fraction measured by NMR is constant at -44°C $< T < -5$°C for 1UBQ/water. The constancy of the mobile water fraction means that when considering the contributions to the thermal effects measured by DSC, only the heat capacities of the constituent phases have to be taken into account. We applied a crude approximation in which we considered the hexagonal ice, unfrozen water, and protein content as three phases, each having individual special heat. No melting occurs in the temperature range examined. This situation gives an opportunity to estimate the specific heat of the hydrate water phase. The heat flow is described by the formula

$$\text{HF} = q\big(m_{\text{water}}(1-x)c_{\text{p,ice}} + m_{\text{water}}xc_{\text{p,hydr}} + m_{\text{protein}}c_{\text{p,protein}}\big), \quad (4)$$

where m_{water} is the mass of solvent water, x is the mobile water fraction measured by NMR, $c_{\text{p,ice}}$ is the specific heat of ice (17), $c_{\text{p,hydr}}$ is the specific heat of hydration water, m_{protein} is the mass of the dissolved protein, and $c_{\text{p,protein}}$ is the specific heat of 1UBQ. Specific heat measurements for UBQ (both native and denatured forms) show substantial temperature dependence above 0°C as measured in aqueous solution (ubiquitin bovine; 10 mM glycine or acetate, pH 2–4) by DSC (39). There are no experimental values published below 0°C to date, to our knowledge. We measured the specific heat of 1UBQ powder between -60 and $+120$°C. Our value of $c_p = 1.40 \pm 0.08$ J·g^{-1}·K^{-1} for 1UBQ powder is equal, within the experimental error, to the literature value of $c_p = 1.33 \pm 0.08$ J·g^{-1}·K^{-1} for 1UBQ in aqueous solution (39), and both were obtained at $+5$°C. In the low-temperature region, where x is constant, the heat capacity of 1UBQ powder changes linearly with temperature as $c_p = 1.19 \pm 0.08$ J·g^{-1}·K^{-1} at -10°C and $c_p = 0.86 \pm 0.08$ J·g^{-1}·K^{-1} at -40°C. We found that the specific heat of the hydration water, $c_{\text{p,hydr}}$, changes between 5.0 ± 0.5 and 5.8 ± 0.5 J·g^{-1}·K^{-1} for 1UBQ/water between -10 and -40°C, where $x = 0.0162 \pm 0.0002$ ($h = 0.395 \pm 0.004$) is constant.

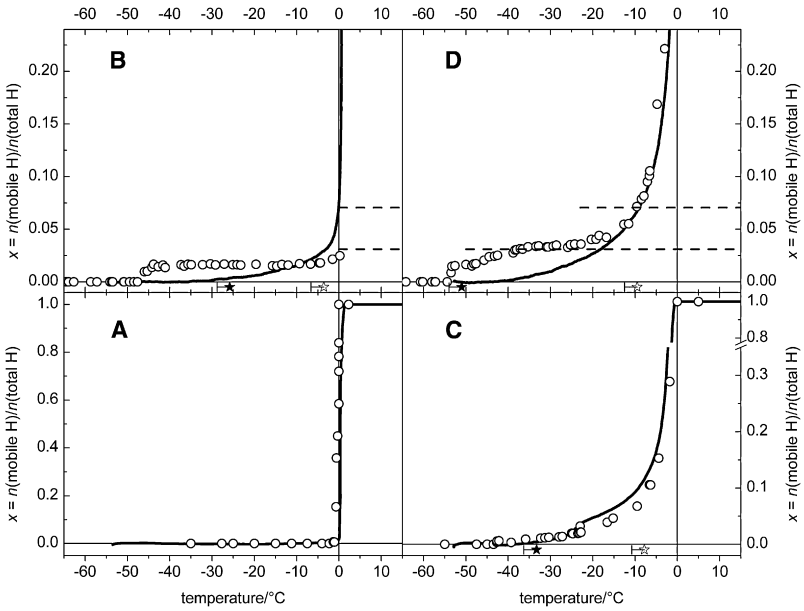

FIGURE 6 Mobile water fractions $x = n$(mobile H)/n(total H) determined from ^{1}H-NMR signal intensities (*circles*) and DSC curves (*lines*) for (*A*) water, (*B*) 41 mg/cm^3 ubiquitin dissolved in water, (*C*) buffer, and (*D*) 41 mg/cm^3 ubiquitin dissolved in buffer. Solid stars denote the lowest temperature where CPMG echoes could be detected and open stars show the lowest temperature where CPMG-echo trains reflected translational diffusion of (water) protons.

These values are higher than the specific heat of water (37) $c_{p,water} = 4.2\ J \cdot g^{-1} \cdot K^{-1}$. The result is not unique in the literature: Yang et al. (40) estimated the partial specific heat of the hydration water of lysozyme, and the result of $5.8\ J \cdot g^{-1} \cdot K^{-1}$ was found in a region of given water coverage.

This unexpected magnitude of $c_{p,hydr}$ is the consequence of assuming that the protein molecule and its hydration water have individual special heat as if they were independent phases. When we repeat the above calculation using the specific heat of water as given for the unfrozen (hydration) water, i.e., $c_{p,hydr} = c_{p,water} = 4.2\ J \cdot g^{-1} \cdot K^{-1}$, and calculate the specific heat of ubiquitin, we get $c_{p,protein} = 1.5 \pm 0.2\ J \cdot g^{-1} \cdot K^{-1}$. This value is again higher than that for the pure substance. These discrepancies show that the protein and its hydration water form a thermodynamic unit and cannot be treated independently.

Specific heat of the hydrated protein

Another approach is to not separate the protein and its hydration shells, but to take them as one entity. We think that this approach is appropriate, because we found that the ^1H longitudinal relaxation rate is identical for the dissolved protein and the hydrate water. As this relaxation process involves radiation-free transitions, the identity of the R_1 values allows the conclusion that the dissolved protein and its hydration water should be considered as one thermodynamic phase. The specific heat of the protein and its hydration water, $c_{p,protein+hydr}$, can be calculated by applying the equation

$$HF = q\left(m_{water}(1-x)c_{p,ice} + \left(m_{water}x + m_{protein}\right)c_{p,protein+hydr}\right). \quad (5)$$

We got an average specific heat for the protein and its hydration water of $c_{p,protein+hydr} = 2.3 \pm 0.1\ J \cdot g^{-1} \cdot K^{-1}$ in the above temperature range of -10 to -40°C for 1UBQ/water. This value for $c_{p,protein+hydr}$ falls into the range limited by the specific heat of solid ubiquitin and liquid water.

Extensive MDSs on *Trichoderma reesei* Endoglucanase III in water and glycerol (10) showed that the protein and the solvent begin to act as a unified and unique system at temperatures where they are functional, i.e., above the temperature of dynamical transition, as we propose for 1UBQ. Moreover, our NMR signal amplitude experiments on Tris buffer (20) showed that buffered protein solutions cannot be interpreted by treating the buffer components (Tris and NaCl) and the protein molecules as independent systems.

CONCLUSIONS

Model independent conclusions

The temperature-dependent multiexperimental approach offered a chance for direct determination of the size and temperature dependence of the water phase in the interfacial region of ubiquitin. The size of the interfacial water phase is represented by the number of mobile protons belonging to water molecules. The slope of the mobile water molecule fraction versus temperature curve gives the homogeneity/heterogeneity of the interfacial region around the protein solutes and the differences in both size and slope in water and buffer solvents. (The homogeneous interfacial region results in zero slope of the x versus T curve.) The hydrogen motion stops/starts at about -73 to -53°C without hysteresis for the protein solutions, in contrast with the buffer, which shows a characteristic difference in transition temperatures in the cooling and heating directions. The low-temperature heat excitation of water molecular motion in the interfacial region (below 0°C, and not at 0°C as in hexagonal ice) indicates that the water molecules are easier to reorient around the protein than in crystalline ice. The hydrogen-bonded structure of the interfacial water-protein surface system is homogeneous in the pure water solutions and heterogeneous in the buffered solutions. The terms homo- and heterogeneity are used here in a thermodynamic sense, referring to differences in the properties of the particular H-bonds.

Model dependent conclusions

The measurements of the low-temperature spectrum widths on the interfacial region protons and temperature values where the CPMG echoes appear and translational diffusion starts, represent a transition to direct relaxation time measurements (M. Bokor, P. Bánki, P. Kamasa, G. Lasanda, P. Tompa, and K. Tompa, unpublished). The line width is connected with the spin-spin relaxation, and the increase in line width toward lower temperatures means the reduction in motional modes of water molecules and finally the slowing down of the molecular reorientation.

The combination of NMR intensity and DSC results gives an estimate of specific heat for the protein-interfacial water entity in aqueous solutions. Analysis of the DSC heat flow traces showed that the protein molecules and their hydration water form one phase in the thermodynamic sense.

Finally, we propose some answers to the questions raised at the end of the section on NMR intensities.

1. The actual size of the hydration shell of the protein molecule could be identified with the number of mobile water molecules for the 1UBQ/water solution at $T < 5$°C. It was found that the hydration shell around the ubiquitin molecule consists of 187 ± 2 water molecules.
2. The big difference in hydration properties when the protein is dissolved in water compared with buffer is due to the surface/structure modification of the protein (41) by the relatively high NaCl concentration in the buffer.
3. The physicochemical background of the substantial change in the NMR intensity curve for buffered solution at about -20°C reveals the ''melting'' of an additional fraction of water, presumably the additional water molecules hydrating the Na^+ and Cl^- ions located near the protein surface (42).

4. The change in the slope at about $-15\ldots-10^{\circ}C$ means a qualitative change in the motion (the appearance of translation) of water molecules at the protein surface.

These two latter features (answers 3 and 4) are missing in the unbuffered solution because they are consequences of the NaCl solute.

The authors acknowledge support from the Hungarian Academy of Sciences and an International Senior Research Fellowship (GR067595) from the Wellcome Trust.

REFERENCES

1. Cooke, R., and J. D. Kuntz. 1974. The properties of water in biological systems. *Annu. Rev. Biophys. Bioeng.* 3:95–126.
2. Rupley, J. A., and G. Carreri. 1991. Protein hydration and function. *Adv. Protein Chem.* 41:37–172.
3. Simonson, T. 2003. Electrostatics and dynamics of proteins. *Rep. Prog. Phys.* 66:737–787.
4. Halle, B. 2004. Protein hydration dynamics in solution: a critical survey. *Philos. Trans. R. Soc. Lond. B Biol. Sci.* 359:1207–1224.
5. Schröder, C., T. Rudas, S. Boresch, and O. Steinhauser. 2006. Simulation studies of the protein-water interface. I. Properties at the molecular resolution. *J. Chem. Phys.* 124:234907.
6. Bizzarri, A. R., and S. Cannistraro. 2002. Molecular dynamics of water at the protein-solvent interface. *J. Phys. Chem. B.* 106:6617–6633.
7. Pal, S. K., J. Preon, B. Bagchi, and A. H. Zewall. 2002. Biological water: femtosecond dynamics of macromolecular hydration. *J. Phys. Chem. B.* 106:12376–12395.
8. Arcangeli, C., A. R. Bizzarri, and S. Cannistraro. 1998. Role of interfacial water in the molecular dynamics-simulated dynamical transition of plastocyanin. *Chem. Phys. Lett.* 291:7–14.
9. Tournier, A. I., and J. C. Smith. 2003. Principal components of the protein dynamical transition. *Phys. Rev. Lett.* 91:208106.
10. Atilgan, C., A. O. Aykut, and A. R. Atilgan. 2008. How a vicinal layer of solvent modulates the dynamics of proteins. *Biophys. J.* 94:79–89.
11. Dill, K. A., T. M. Truskett, V. Vlachy, and B. Hribar-Lee. 2005. Modeling water, the hydrophobic effect, and ion solvation. *Annu. Rev. Biophys. Biomol. Struct.* 34:173–199.
12. Tompa, P. 2002. Intrinsically unstructured proteins. *Trends Biochem. Sci.* 27:527–533.
13. Dyson, H. J., and P. E. Wright. 2005. Intrinsically unstructured proteins and their functions. *Nat. Rev. Mol. Cell Biol.* 6:197–208.
14. Bokor, M., V. Csizmók, D. Kovács, P. Bánki, P. Friedrich, et al. 2005. NMR relaxation studies on the hydrate layer of intrinsically unstructured proteins. *Biophys. J.* 88:2030–2037.
15. Csizmók, V., M. Bokor, P. Bánki, É. Klement, K. F. Medzihradszky, et al. 2005. Primary contact sites in intrinsically unstructured proteins: the case of calpastatin and microtubule-associated protein 2. *Biochemistry.* 44:3955–3964.
16. Tompa, P. 2005. The functional benefits of protein disorder. *J. Mol. Struct. THEOCHEM.* 666–667:361–371.
17. Derbyshire, W. 1982. The dynamics of water in heterogeneous systems with emphasis on subzero temperatures. *In* Water. A Comprehensive Treatise, volume 7: Water and Aqueous Solutions at Subzero Temperatures. F. Franks, editor. Plenum Press, New York.
18. Kuntz, I. D., T. S. Brassfield, G. D. Law, and G. V. Purcell. 1969. Hydration of macromolecules. *Science.* 163:1329–1331.
19. Kuntz, I. D. 1971. Hydration of macromolecules. III. Hydration of polypeptides. *J. Am. Chem. Soc.* 93:514–516.
20. Tompa, P., P. Bánki, M. Bokor, P. Kamasa, D. Kovács, et al. 2006. Protein-water and protein-buffer interactions in the aqueous solution of an intrinsically unstructured plant dehydrin: NMR intensity and DSC aspects. *Biophys. J.* 91:2243–2249.
21. Hahn, E. L. 1950. Spin echoes. *Phys. Rev.* 80:580–594.
22. Carr, H. Y., and E. M. Purcell. 1954. Effects of diffusion on free precession in nuclear magnetic resonance experiments. *Phys. Rev.* 94: 630–638.
23. Meiboom, S., and D. Gill. 1958. Modified spin-echo method for measuring nuclear relaxation times. *Rev. Sci. Instrum.* 29:688–691.
24. Powles, J. G., and P. Mansfield. 1962. Double-pulse nuclear-resonance transients in solids. *Phys. Lett.* 2:58–59.
25. Slichter, C. P. 1990. Principles of Magnetic Resonance, 3rd ed. Springer Verlag, Berlin.
26. Abragam, A. 1961. The Principles of Nuclear Magnetism. Clarendon, Oxford, United Kingdom. 424.
27. Tompa, K., P. Bánki, M. Bokor, G. Lasanda, and J. Vasáros. 2003. Diffusible and residual hydrogen in amorphous Ni(Cu)–Zr–H alloys. *J. Alloy. Comp.* 350:52–55.
28. Mallamace, F., S.-H. Chen, M. Broccio, C. Corsaro, V. Crupi, et al. 2007. Role of the solvent in the dynamical transitions of proteins: the case of the lysozyme-water system. *J. Chem. Phys.* 127:045104.
29. Kamasa, P., M. Bokor, M. Pyda, and K. Tompa. 2007. DSC approach for the investigation of mobile water fractions in aqueous solutions of NaCl and Tris buffer. *Thermochim. Acta.* 464:29–34.
30. Kamasa, P. 2004. Technical Note, Application of DPSD to DSC; Research Institute for Solid State Physics and Optics, Hungarian Academy of Sciences: Budapest, http://www.szfki.hu./~kamasa/DPSDDSC1.htm.
31. Gregory, R. B. 1995. Protein-Solvent Interactions. CRC, New York.
32. Teeter, M. M. 1991. Water-protein interactions: theory and experiment. *Annu. Rev. Biophys. Biophys. Chem.* 20:577–600.
33. Grüner, G., and K. Tompa. 1968. Molekuláris mozgások vizsgálata szilárdtestekben NMR módszerrel. *Kémiai Közlemények.* 30:315–356.
34. Russo, D., G. L. Hura, and J. R. D. Copley. 2007. Effects of hydration water on protein methyl group dynamics in solution. *Phys. Rev. E Stat. Nonlin. Soft Matter Phys.* 75, 040902 (R).
35. Curtis, J. E., M. Tarek, and D. J. Tobias. 2004. Methyl group dynamics as a probe of the protein dynamical transition. *J. Am. Chem. Soc.* 126:15928–15929.
36. Ibarra-Molero, B., G. I. Makhatadze, and J. M. Sanchez-Ruiz. 1999. Cold denaturation of ubiquitin. *Biochim. Biophys. Acta.* 1429: 384–390.
37. Lide D. R., editor. (2001–2002). CRC Handbook of Chemistry and Physics, 82nd ed. CRC Press, New York.
38. Wood, R. H., R. A. Rooney, and J. N. Braddock. 1969. Heats of dilution of some alkali metal halides in deuterium oxide and water. *J. Phys. Chem.* 73:1673–1678.
39. Makhatadze, G. I. 1998. Heat capacities of amino acids, peptides and proteins. *Biophys. Chem.* 71:133–156.
40. Yang, P., and J. A. Rupley. 1979. Protein-water interactions: heat capacity of the lysozyme-water system. *Biochemistry.* 18:2654–2661.
41. Pegram, L. M., and M. T. Record, Jr. 2008. Thermodynamic origin of Hofmeister ion effects. *J. Phys. Chem. B.* 112:9428–9436.
42. Finer, E. G., and A. Darke. 1974. Phospholipid hydration studied by deuteron magnetic resonance spectroscopy. *Chem. Phys. Lipids.* 12:1–16.